MICROCOPY RESOLUTION TEST CHART
NATIONAL BUREAU OF STANDARDS-1963

Unclassified

AD-A190 310

DOCUMENTATION PAGE

Form Approved
OMB No. 0704-0188

SECURITY CLASSIFICATION	1b RESTRICTIVE MARKINGS
Unclassified	

2a SECURITY CLASSIFICATION AUTHORITY	3 DISTRIBUTION/AVAILABILITY OF REPORT
2b DECLASSIFICATION/DOWNGRADE SCHEDULE JAN 1 9 1988	Approved for public release; distribution is unlimited

4 PERFORMING ORGANIZATION REPORT NUMBER(S)	5 MONITORING ORGANIZATION REPORT NUMBER(S)
D	AFOSR·TR· 87-1759

6a NAME OF PERFORMING ORGANIZATION	6b OFFICE SYMBOL (If applicable)	7a NAME OF MONITORING ORGANIZATION
Massachusetts Institute of Technology-Plasma Fusion Center		AFOSR/NA

6c ADDRESS (City, State, and ZIP Code)	7b ADDRESS (City, State, and ZIP Code)
167 Albany Street Cambridge, MA 02139	Building 410, Bolling AFB DC 20332-6448

8a NAME OF FUNDING/SPONSORING ORGANIZATION	8b OFFICE SYMBOL (If applicable)	9 PROCUREMENT INSTRUMENT IDENTIFICATION NUMBER
AFOSR/NA		AFOSR 84-0190

8c ADDRESS (City, State, and ZIP Code)	10 SOURCE OF FUNDING NUMBERS			
Building 410, Bolling AFB DC 20332-6448	PROGRAM ELEMENT NO	PROJECT NO	TASK NO	WORK UNIT ACCESSION NO
	61102F	2308	A1	

11 TITLE (Include Security Classification)

(U) PLASMA-GAS INTERACTION STUDIES IN A HYBRID PLUME PLASMA ROCKET

12 PERSONAL AUTHOR(S)
F. R. Chang-Diaz, T. F. Yang

13a TYPE OF REPORT	13b TIME COVERED	14 DATE OF REPORT (Year, Month, Day)	15 PAGE COUNT
Annual	FROM 9/1/86 TO 8/30/87	1987 September 30	30

16 SUPPLEMENTARY NOTATION

17	COSATI CODES		18 SUBJECT TERMS (Continue on reverse if necessary and identify by block number)
FIELD	GROUP	SUB-GROUP	Hybrid Plume, Plasma propulsion Tandem mirror

19 ABSTRACT (Continue on reverse if necessary and identify by block number)

This report discusses the progress in the fluid modeling of a hybrid plume plasma rocket and the heating of plasma in a tandem mirror device. In the theoretical area three tasks have been accomplished: (1) A major advance has been made in the development of a numerical method for solving the time dependent fluid equations for both ions and electrons in the plasma. (2) A mathematical model has been formulated for studying the radio frequency heating of the hot plasma in cylindrical geometry. (3) An analysis on the performance characteristics of the hybrid plume rocket has been carried out. Under the funding of the instrumentation program the component fabrication is in progress. The coils have been delivered.

20 DISTRIBUTION/AVAILABILITY OF ABSTRACT	21 ABSTRACT SECURITY CLASSIFICATION
☒ UNCLASSIFIED/UNLIMITED ☒ SAME AS RPT ☐ DTIC USERS	Unclassified

22a NAME OF RESPONSIBLE INDIVIDUAL	22b TELEPHONE (Include Area Code)	22c OFFICE SYMBOL
Dr Mitat Birkan	(202) 767-4937	AFOSR/NA

DD Form 1473, JUN 86   Previous editions are obsolete   SECURITY CLASSIFICATION OF THIS PAGE

Unclassified

PROGRESS REPORT

to the

Air Force Office of Scientific Research

by

F. R. Chang-Diaz*

T. F. Yang

September 1987

D. B. Montgomery

_____

Associate Director

R. C. Davidson

_____

Director

*Astronaut Office of the Johnson Space Center

1

1.0 Summary

The main effort this year is to understand the physics of the hybrid plume and heating of the plasma in a tandem mirror device. In the theoretical area three tasks have been accomplished: (1) A major advance has been made in the development of a numerical method for solving the time dependent fluid equations for both ions and electrons in the plasma. Realistic physical properties and nonuniform magnetic fields were considered. (2) A mathematical model has been formulated for studying the radio frequency heating of the hot plasma in cylindrical geometry. (3) An analysis on the performance characteristics of the hybrid plume rocket has been carried out.

Under the funding of the instrumentation program some effort has been dedicated to the construction of a tandem mirror device. The component fabrication began in May after several months of contract negotiations since authorization of the fund, and is progressing well.

To obtain a quick but crucial understanding of the hybrid plume concept, a steady state fluid model code for studying the interaction of hot plasma with neutral gas jet was developed in past years. In that code a uniform magnetic field was assumed. It was found that the transition region has been formed and an exhaust duct can be protected by surrounding the hot plasma with a supersonic gas jet. Therefore the simplified version of the computation code has fulfilled the purpose of verifying the hybrid plume concept. To further understand the detailed flow dynamics of the exhaust. a time dependent fluid model for plasma in a general magnetic field configuration has to be solved with realistic physical assumption. To develop such a model was the task undertaken this year. After overcoming many difficult numerical instability problems, a fundamental two dimensional time dependent code is now operational. More importantly, the plasma is now treated as two fluids, the ions and electrons, instead of one fluid used in the previous code. However, many difficult problems have to be worked out in order to use the code in a parametric study. The outflow boundary has to be properly treated. The neutral gas jet, atomic reactions and radiation have to be included. Solving the outflow boundary problem will

2

be the next major task for the coming year.

Previously a slab model for studying the ion cyclotron range of frequency heating was developed. It was shown that the heating efficiency can be improved by optimizing the antenna loading impedance. The loading impedance on the antenna was found parametrically dependent on the magnetic field strength. the distance between the antenna and vessel wall. the plasma density and the dimension of the antenna. Currently. a more accurate and realistic cylindrical model for the power absorption in the plasma has been formulated analytically. In order to learn the heating mechanism and to optimize the efficiency, we would like to obtain an explicit parametric dependence of the power absorption in the plasma on machine and plasma parameters.

For the construction of the tandem mirror device the central cell coils and one mirror coil have been delivered. The liquid nitrogen coil casings are in the process of being fabricated. The fabrications of the vacuum vessel is progressing well. The assembly of the device is expected in November.

2.0 Concept

It would be useful to reintroduce the concept in this section and to investigate the physical problems in the next section. A hybrid plume rocket is one where the macroscopic properties of the exhaust fluid (i.e.. temperature. density. fluid velocity, etc.) exhibit a drastic variation from one radial position to another 1,5. In a hybrid plume rocket, the temperature at the core of the exhaust is extremely high; whereas, near the edge. it is quite low. In fact, the variation in temperature from the plume centerline to the outside can be many order of magnitude. while the exhaust fluid at the center is a fully ionized plasma (at .5 to 1 keV). at the edges it actually becomes a neutral gas (at .1 to .3 eV). As a result. the cool flow at the edges relaxes the heating constraints on the nozzle material while the hot central core preserves and even enhances the allowable power density and specific impulse of the device. The concept has a potential application in rocket propulsion.

3

Figure 1 shows the tandem mirror device with a hot plasma column. One could envision a very hot plasma exhaust surrounded by an annular layer of insulating gas. The hot plasma is generated by a two stage process involving an initial source of cool dense plasma injected axially into a straight tandem mirror device from the left end. Once magnetically confined, the plasma can be heated to the keV regime by microwave injection. The plasma then escapes through one end into an exhaust nozzle on the right end. The hybrid plume is formed slightly downstream of the nozzle throat, as the hypersonic annular gas layer is injected and a stable boundary is established.

The rocket propulsive efficiency η is in free space and in the absence of gravitational effects is $\eta_p = \frac{2v/u}{1-(v/u)^2}$ in terms of vehicle velocity v and exhaust velocity u. Optimum efficiency occurs when $v = u$. The hybrid plume would produce a variable specific impulse I_{sp} which allows the engine to be optimally tuned for all phases of flight. The terminal velocity of the hybrid is nearly ten times the initial velocity when reaching burnup.

3.0 Physical Problems

The physics of high temperature hydrogenic plasmas, interacting with hypersonic gas jets are not well understood. Analytical and numerical modeling of these interactions requires the simultaneous, self-consistent solution of particle, momentum and energy transport equations for each particle species. Therefore, the crucial area of investigation *pertaining to the physics of hybrid plumes is the numerical modeling of the plasma/gas interaction in the exhaust.*

The numerical modeling results have to be tested experimentally. The plasma conditions achieved in the fusion program have exceeded the need for propulsion purposes. However, the devices used for fusion experiments are usually large because the purpose is aimed at power reactors. To find a light and compact device suitable for propulsion has to be carefully investigated. The basic plasma physics for the compact device and control of plasma flow are not known and need extensive experimental study.

4.0 Time Dependent Fluid Modeling

As discussed in the summary, the parametric study obtained by the code developed previously has shown the viability of the hybrid plume rocket 2.3. The interactions between the neutral gas jet and plasma have been demonstrated to form the transition region required to form the hybrid plume. Also, with varying the amount of neutral gas introduced into the system, one can modulate the central core temperature. This is an important parameter in controlling the plasma flow. The next critical issue to address is the detailed flow dynamics of the hybrid plume concept. Specifically, whether the plasma flow will detach from the nozzle and produce usable thrust at high I_{sp}. Preliminary results show that the neutral gas jet can provide the momentum needed to cause the plasma to form closed magnetic flux surfaces which will flow out the exhaust duct like a ring and eventually disconnect from the main field line. This phenomena will be referred to as field line disconnection in this write-up.

The previous code used a cylindrically symmetric duct with the plasma flowing axially and diffusing radially. This assumption was used to understand the principle mechanisms involved with the hybrid plume concept and to study the feasibility of the hybrid plume concept. The code was not designed to specifically study the disconnection process. The magnetic field was assumed constant in time and essentially constant in space (a modified diffusion coefficient was used to model the weakly diverging magnetic field). The code calculated density, n, temperature T, and axial velocity V_z. The radial velocity was not needed because of the diffusion model used. This limited the interactions between the neutral gas and plasma to the diffusion time scale. In reality, the plasma will physically flow radially along the diverging field line. In a real nozzle, V_r will be important. Depending on the strength of the interactions between the neutral gas jet and the plasma, the plasma may cling to the field lines and actually reverse directions as the magnetic field bends around the edge of the nozzle. Also, the dynamics of the flow can alter the local magnetic field, so the field would be non-stationary. Thus to accurately model the hybrid plume, and the separation of the plasma from the field lines, one must improve the numerical model significantly.

5

A simple mass and momentum balance argument shows that the neutral gas jet can provide the momentum needed to drive the disconnection and separate the plasma flow from the field lines. Since the neutral gas jet is located near the wall of the exhaust, the interaction region will form downstream from this point. The magnetic field will be falling off rapidly in this region. Thus, the momentum required in the neutral gas jet can be small while still driving the reconnection process. A potential sequence is shown in Fig. 2. The neutral gas jet flows axially down a duct immersed in a diverging magnetic field. As the neutral gas jet becomes ionized, its resistivity and flow profile modify the magnetic field and the remaining plasma flow. This allows the flow to disconnect from the nozzle and continue down the duct. This detachment mechanism is presently under study and will be one of the new modifications to the present code.

Our current effort has been to improve the computational model to include a more realistic magnetic field geometry. Further refinements in a physics of the interactions between the neutral jet and plasma will also be included. In an actual machine it is not obvious that a true steady state will be obtained (periodic operation can be envisioned). The new model will be time dependent, two dimensional in space, and three-dimensional in velocity and electric and magnetic fields. For fully ionized plasma the ion and electron density are approximately equal. These two species of particles have different mobility and should be treated as separate fluids in an open system like our case. The complexity is double that of the single fluid treatment. However, the electron is much lighter than the ion. It is reasonable to make the zero-electron mass assumption. A zero-electron-mass hybrid code is being developed. It is a two-fluid, two dimensional (r and z), quasi-neutral code. This code can adequately model the complex flow and evolution on the hybrid plume dynamics.

With zero mass the electron momentum equation reduces to

$$\mathbf{E} \quad \frac{\nabla \rho T_e}{e\rho} \quad \frac{\mathbf{u_e} \times \mathbf{E}}{c} \cdot \eta \cdot \mathbf{J} . \tag{1}$$

where $\mathbf{E}$ is the electric field vector. ρ is the particle density, T_e is the electron temperature, e is the charge of an electron, $\mathbf{u_e}$ is the electron velocity vector. $\mathbf{E}$ is the magnetic field vector,

6

η is the resistivity tensor, and $\mathbf{J}$ is the current density vector. The fluid equations for ions are the same as reported previously. Using the Darwin limit of Maxwell's equations and also the magnetic vector potential $\mathbf{A}$, the electron momentum equation can be rewritten in a form for the time evolution of $\mathbf{A}$,

$$\dot{\mathbf{A}} = c\frac{\nabla p_e}{\epsilon \rho} - \mathbf{u_e} \times (\nabla \times \mathbf{A}) - \frac{c^2}{4\pi}\eta \cdot \nabla \times \nabla \times \mathbf{A} . \qquad (2)$$

One actually only needs the theta component of the above equation and one can obtain both B_r and B_z. A similar transformation results in an equation for the time evolution of B_θ.

The electron fluid velocities are calculated according to the currents. In other words,

$$U_{er} = U_{ir} - \frac{c}{4\pi\epsilon\rho}\frac{\partial B_\theta}{\partial z} ,$$

$$U_{e\theta} = U_{i\theta} - \frac{c}{4\pi\epsilon\rho}\nabla^2 A_\theta , \qquad (3)$$

$$U_{ez} - U_{iz} - \frac{c}{4\pi\epsilon\rho}\frac{1}{r}\frac{\partial(rB_\theta)}{\partial r} .$$

All that is needed to complete the picture are the fluid quantities, and they are calculated using the normal fluid equations for mass, velocity, and temperature.

The goal of the current development will be the ability to model the detailed behavior of the plasma gas flow in a complex magnetic field. This is important because the plasma will tend to cling to the field lines (which diverge), while the neutral gas will tend to go straight. The bulk flow will be some complicated balance between the two. The higher the plasma temperature, and thus higher potential I_{sp}, the more the plasma flow will be frozen the field lines. To obtain realistic thrust predictions, detailed characteristics of the flow field must be determined. The code solves for the evolution of mass, momentum, energy, and magnetic field. The plasma equations are solved explicitly, with the coupled field equations solved implicitly.

5.0 Plasma Heating

Progress made in ICRF heating this year includes the theoretical study, the power absorption of the plasma, and design of the power systems for ICRF heating. An engineering design of the rf power transmission systems was performed with the assistance of the radio frequency power transmitter expert from the Alcator group.

On the theoretical side, further work was done in the optimization of antenna heating. Last year, power absorption calculations were performed in a slab Cartesian geometry. While the results obtained using Cartesian geometry proved insightful, they are not very physically applicable. The geometry of the device is such that the free space wavelength of the RF waves generated λ are much larger than the physical size of the plasma and or the device a. Since the Cartesian approach means that the plasma is in effect of infinite size such that the geometric effects of its cylindrical shape do not affect the results, it means that we need $\lambda \gg a$, which is not the case here. So while the calculations obtained using slab geometry are useful in that they yield intuitive results, they are not a very effective model of the physical conditions of the experiment. This year, calculations using the cylindrical model are performed and are being examined. Collisions are included to examine what effects collisions may have on the heating of the plasma. In the future, finite temperature effects will also be introduced to better model a laboratory plasma.

The electromagnetic field structure inside a cylindrical plasma was calculated and examined to maximize the power injected into the plasma by the antenna.

Define:

$$I_{nr} = I_n(\nu r) \ . \tag{4}$$

$$J_{n1r} = J_n(\nu_1 r) \ . \tag{5}$$

$$J_{n2r} = J_n(\nu_2 r) \ . \tag{6}$$

$$y_2 = \frac{i\omega\mu_0 k_z D}{P(k_z^2 - k_0^2 S) - Sk_{r1}^2} \ . \tag{7}$$

and

$$z_1 = \frac{i\omega\epsilon_0 k_z P D}{S(k_{r2}^2 - k_z^2) - RLk_0^2} \ . \tag{8}$$

From Maxwell's equations. the fields inside a cylinder can be calculated to be:

Region I. (Plasma Region)

$$H_z(r) = H_1 J_{n1r} - z_1 E_2 J_{n2r} , \tag{9}$$

$$E_z(r) = E_2 J_{n2r} - y_2 H_1 J_{n1r} , \tag{10}$$

Region II. (Vacuum Region)

$$H_z(r) = H_2^- I_{nr} - H_2^- K_{nr} , \tag{11}$$

$$E_z(r) = E_2^- I_{nr} - E_2^- K_{nr} , \tag{12}$$

Region III. (Vacuum Region)

$$H_z(r) = H_3^+ I_{nr} + H_3^- K_{nr} , \tag{13}$$

$$E_z(r) = E_3^- I_{nr} + E_3^- K_{nr} . \tag{14}$$

The coefficients of the fields can be found subject to the following boundary conditions:

B.C.

(1) At r=c,

$$E_\theta = E_z = 0 . \tag{15}$$

$$H_r = 0 . \tag{16}$$

(2) At r=b

$$E_{\theta II} = E_{\theta III} , \tag{17}$$

$$E_{zII} = E_{zIII} , \tag{18}$$

$$H_{zII} = H_{zIII} - J_{s\theta} . \tag{19}$$

$$H_{\theta III} = H_{\theta II} - J_{sz} . \tag{20}$$

(3) At r =a

9

$$E_{\theta II} = E_{\theta III} \ . \tag{21}$$

$$E_{zII} = E_{zIII} \ . \tag{22}$$

$$H_{\theta II} = E_{\theta III} \ . \tag{23}$$

$$H_{zII} = E_{zIII} \ . \tag{24}$$

After calculations were performed to find the field coefficients, the power injected into the plasma can be evaluated by

$$\vec{S} = \frac{dP}{dk_z} = \vec{E} \times \vec{H}^* \ , \tag{25}$$

and

$$P_{plasma} = \int_{-\infty}^{\infty} \frac{dP}{dk_z} dk_z \ . \tag{26}$$

Define elements of the dielectric tensor (including collisions of collision frequency ν_c):

$$S = 1 - \Sigma_\alpha \frac{\omega_{p\alpha}^2}{\omega^2 - \Omega^2} \left[1 - i \frac{\nu_c}{\omega} \left(\frac{\omega^2 - \Omega^2}{\omega^2 - \Omega^2} \right) \right] \ . \tag{27}$$

$$D = \Sigma_\alpha \frac{\omega_{p\alpha}^2 \Omega}{\omega(\omega^2 - \Omega^2)} - i \frac{2\omega_{p\alpha}^2 \nu_c \Omega}{(\omega^2 - \Omega^2)} \ , \tag{28}$$

and

$$P = 1 - \Sigma_\alpha \frac{\omega_{p\alpha}^2}{\omega^2} \left(1 - i \frac{\nu_c}{\omega} \right) \ . \tag{29}$$

Define:

$$\mathcal{L} \equiv S(k_{r2}^2 - k_z^2) - RLk_0^2 \ , \tag{30}$$

$$\approx \frac{k_z^2(2S - n_z^2)}{(n_z^2 - S)} \ . \tag{31}$$

$$\Psi \equiv k_z^2 - k_0^2 S \ , \tag{32}$$

$$\mathcal{F}_0 \equiv \frac{\triangle_{b'c'}}{\triangle_{b'b}} \frac{K_{na} - K_{na}' \triangle_{ac'}}{\triangle_{a'c'} J_{n2a} - \frac{\nu \nu_\perp}{\Psi} \triangle_{ac'} J_{n2a}} \ . \tag{33}$$

10

$$\mathcal{P}_2 \equiv - K_{na} K'_{nc} \frac{\triangle_{bc}}{\triangle_{ac}} - \triangle_{bc} K_{na} K'_{nc}$$
$$- \frac{b}{a}(-\triangle_{b'c'} K_{na} K_{nc} K'_{nc} - \triangle_{b'c'} K_{na} K_{nc}) \ . \tag{34}$$

$$\mathcal{P}_3 \equiv 1 - \frac{\Psi^2 - D^2 k_0^4}{\Psi \nu^2} \ , \tag{35}$$

$$\mathcal{P}_1 \equiv 1 - \frac{\Psi \nu^2}{\Psi^2 - D^2 k_0^4} \ , \tag{36}$$

$$\mathcal{G}_0 \equiv \frac{\triangle_{ac'} \triangle_{bc}(\frac{1}{\nu b} - 1)}{\triangle_{a'c'} J_{n2a} - \frac{\nu \nu_1}{\Psi} J_{n2a} \triangle_{ac'}} \ . \tag{37}$$

$$\mathcal{A}_1 \equiv \frac{\mathcal{P}_2 k_z n}{\nu^2 b K'_{nc}} \ . \tag{38}$$

$$\mathcal{A}_2 \equiv \triangle_{bc} K'_{na}(1 - \frac{\triangle_{ac'} K_{na}}{\nu b}) \ , \tag{39}$$

and

$$\mathcal{K}_1 \equiv \frac{a S k_0^2 (n_z^2 - S)}{k_z \mathcal{P}_3 n K_{nc} \triangle_{b'b}} \ . \tag{40}$$

The results obtained from the analysis yields:

$$E_z(r = a) = \frac{i k_0^2}{\omega \epsilon_0 P} \left\{ \frac{S J_{n2a} a(2S - n_z^2)(\mathcal{A}_1 J_{s\theta} - \mathcal{A}_2 J_{sz})}{n D \triangle_{b'b} K_{nc} J_{n2a} \mathcal{P}_3} \right.$$
$$\left. - \frac{k_z D J_{n1r}(\mathcal{F}_0 J_{s\theta} - \mathcal{G}_0 J_{sz} \frac{n k_z}{a k_0^2})}{(k_z^2 - k_0^2 S - S k_{r1}^2)} \right\} \ . \tag{41}$$

$$H_z(r = a) = J_{s\theta} \left[J_{n1a} \mathcal{F}_0 - \frac{k_z \mathcal{A}_1 S k_0^2 (2S - n_z^2) a J_{n2a}}{\mathcal{L} \mathcal{P}_3 n \triangle_{b'b} K_{nc} J_{n2a}} \right]$$
$$- J_{sz} \left[\frac{\mathcal{G}_0 n k_z J_{n1a}}{a k_0^2} - \frac{a k_z \mathcal{A}_2 S k_0^2 (2S - n_z^2) J_{n2a}}{\mathcal{P}_3 \mathcal{L} n \triangle_{b'b} K_{nc} J_{n2a}} \right] \ . \tag{42}$$

$$E_\theta(r - a) = \frac{i k_0^2 J_{n1a} \nu_1}{\Psi \omega \epsilon_0} \left\{ J_{s\theta}(\mathcal{F}_0 + \frac{a S k_0^2 (2S - n_z^2) \mathcal{A}_1 k_z \nu_2 J'_{n2a}}{n \triangle_{b'b} K_{nc} \mathcal{P}_3 \mathcal{L}}) \right.$$
$$\left. + J_{sz}(\frac{n k_z \mathcal{G}_0}{a k_0^2} - \frac{S k_0^2 (2S - n_z^2) a k_z \mathcal{A}_2 \nu_2 J'_{n2a}}{n \triangle_{b'b} K_{nc} \mathcal{P}_3}) \right\} \ , \tag{43}$$

11

and

$$H_\theta(r = a) = \frac{\Psi k_z n J_{n1a}}{a(\Psi^2 - D^2 k_0^4)} \left\{ J_{s\theta}\left(\mathcal{F}_0 - \frac{Sak_z k_0^2(2S - n_z^2)\mathcal{A}_1}{\mathcal{L}J_{n1a}n \triangle_{b'b} K_{nc}\mathcal{P}_3}\right) \right.$$
$$\left. - J_{sz}\left(\frac{nk_z \mathcal{G}_0}{ak_0^2} + \frac{k_z aS k_0^2(2S - n_z^2)\mathcal{A}_2}{\mathcal{L}J_{n1a}n \triangle_{b'b} K_{nc}\mathcal{P}_3}\right) \right\} . \qquad (44)$$

The radial power flux is found by

$$\mathbf{S}_r = \frac{1}{2}\mathbf{E} \times \mathbf{H}^*$$
$$= E_\theta H_z^* - E_z H_\theta^* . \qquad (45)$$

Assuming a loop antenna, the formula for the power flux through the plasma's edge (r=a) is found to be:

$$S_r = \frac{ik_0^2 J_{n2a}{}^2}{\omega\epsilon_0}\left[\mathcal{F}_0{}^2\left(\frac{\nu_1}{\Psi} - \frac{k_z^2 \Psi D n}{aP(\Psi^2 - D^2 k_0^4)(k_z^2 - k_0^2 S + \frac{S}{P}k_{r1}^2)}\right)\right.$$
$$- \mathcal{F}_0 \mathcal{A}_1\left(\frac{\nu_1 \mathcal{K}_1}{\Psi}\left(1 + \frac{\nu_2 J'_{n2a}}{\nu_1 J_{n2a} J_{n2a}}\right) + \frac{kz^4 k_0^2 S^*(2S - n_z^2)\Psi D}{\mathcal{L}J_{n2a}\triangle_{b'b}K_{nc}\mathcal{P}_3 P(\Psi^2 - D^2 k_0^4)(k_z^2 - k_0^2 S - \frac{S}{P}k_{r1}^2)}\right.$$
$$\left. - \frac{k_z^3 \Psi S(2S - n_z^2)}{P(\Psi^2 - D^2 k_0^4)\triangle_{b'b}K_{nc}J_{n2a}\mathcal{P}_3}\right) \qquad (46)$$
$$\left. - \mathcal{A}_1{}^2\left(\frac{\mathcal{K}_1{}^2 \nu_2 J'_{n2a}}{\Psi J_{n2a} J_{n2a}} - \frac{k_z^3 \Psi n Dak_0^2 S^2(2S - n_z^2)(2S^* - n_z^2)}{J_{n2a}P^2(\Psi^2 - D^2 k_0^4)(k_z^2 - k_0 S - \frac{s}{P}k_{r1}^2)n\mathcal{L}^* J_{n2a}\triangle_{b'b}{}^2\mathcal{P}_3^2}\right) \right] .$$

The real power flux absorbed by the plasma can then be found by taking the real part of the radial Poynting flux, Re(S_r). The total power into the plasma can then be found by integrating the Poynting Flux with respect to k_z.

In future work, the cylindrical analysis will be extended to warm plasmas so that a more realistic model of a laboratory plasma can be obtained and compared to future experimental results.

12

6.0 Performance Characteristics of the Hybrid Plume Rocket

This discussion focuses on the basic physical laws governing the operation and optimization of the hybrid plume. It assumes a suitable power source can be provided which can deliver a power level, P, to the plasma. Microwave and other rf efficiencies are not discussed here as they are experimental quantities which need to be measured in a real device. As such, these values neither add nor subtract to the physics to be discussed here. With these considerations, the basic momentum and energy relationships as they would apply to the hybrid plume engine will not be explored.

6.1 Basic Assumptions

The basic momentum balance for a rocket in free space and assuming no gravitational effects can be expressed as

$$v' = -\frac{um'}{m}$$ (47)

where v' and m' are time derivations of the vehicle velocity with respect to a fixed point (i.e., the Earth) and rocket total mass respectively. u is the exhaust velocity as measured in the frame of the rocket.

The rocket exhaust power flow, P, can also be expressed as

$$P = m'\frac{u^2}{2}.$$ (48)

Also, the various masses can be related a follows:

$$m(t) = m_0 m_f(t)$$ (49)

where m_0 is the total mass of rocket and fuel at $t = 0$, and $m_f(t)$ is the total mass of fuel exhausted through the nozzle at time t.

We not define the propulsive efficiency of the engine, η_p, as the fraction of the total power available which is converted to vehicle kinetic power. That is,

$$\eta_p \equiv \frac{Tv}{Tv + \frac{m'}{2}(v - u)^2}$$ (50)

13

where T is the instantaneous thrust, $m'u$ and the quantity $m'(v - u)^2/2$ represents the residual power which is carried out by the exhaust. In terms of the velocity ratio (v/u), Eq. (50) can be recast as follows:

$$\eta_p = \frac{2\frac{v}{u}}{\left[1 - \left(\frac{v}{u}\right)^2\right]} \ . \tag{51}$$

Equation (51) is shown plotted in Fig. 5 as a function of the velocity ratio. It can be seen that the optimum occurs when $v = u$.

With the above requirement, one can now rewrite Eqs. (47) and (48) in terms of v along; that is

$$v' = -\frac{vm'}{m} \tag{52}$$

and

$$2P = v^2 m' \ . \tag{53}$$

Equation (52) can be integrated to give

$$\int_{v_0}^{v} \frac{dv}{v} = -\int_{m_0}^{m} \frac{dm}{m} \tag{54}$$

so that

$$\frac{v}{v_0} = \frac{m_0}{m} \tag{55}$$

and, defining the mass fraction γ as m_f/m_0

$$v = v_0 \left(\frac{1}{1 - \gamma}\right) \ . \tag{56}$$

Equation (56) is shown plotted in Fig. 6 as v/v_0 as a function of γ. For comparison, the same velocity ratio profile for a constant I_{sp} chemical rocket, with $u/v_0 = .5$ is shown as a dashed curve. One can view this result in two ways; first, for the same mass fraction, the hybrid plume rocket can achieve significantly greater velocities, and second, for the same terminal velocity the hybrid plume rocket represents a substantially lower mass fraction and hence a substantially greater payload capacity.

14

In this regard. it must also be pointed out that a constant, high I_{sp} rocket is also attractive. However, the hybrid plume concept presented here has some added advantages over even this latter approach. This will be shown next.

6.2   Rocket Performance With Variable I_{sp}

In order to be desirable the hybrid plume rocket must also have sufficient acceleration. Accordingly. it is important to obtain a relationship for v as a function of time. Such a relationship will be derived next. Using Eqs. (55) and (53) one can write

$$\frac{2P}{(v_0 m_0)^2} dt = \frac{dm}{m^2} \ . \tag{57}$$

Integrating this expression

$$\frac{2Pt}{(v_0 m_0)^2} = -\int_{m_0}^{m} \frac{dm}{m^2} \tag{58}$$

where the negative sign has been introduced to account for the mass decreasing. The result after integrating is

$$\frac{1}{m_0} + \frac{2Pt}{(v_0 m_0)^2} = \frac{1}{m} \tag{59}$$

and solving for m as a function of time gives

$$m(t) = \frac{1}{\frac{1}{m_0} + \frac{2Pt}{(v_0 m_0)^2}} \ . \tag{60}$$

From this expression one can calculate the burnup time τ which defines the dry mass of the rocket m_r.

$$\tau \equiv \left(1 - \frac{m_r}{m_0}\right) \frac{v_0^2 m_0^2}{2P m_r} \ . \tag{61}$$

Equations (55) and (60) can now be combined to obtain velocity as a function of time:

$$v(t) = v_0 - \frac{2Pt}{v_0 m_0} \tag{62}$$

and an additional integration yields the distance χ as a function of time:

$$\chi(t) = v_0 t - \frac{Pt^2}{v_0 m_0} \ . \tag{63}$$

15

Note from Eqs. (62) and (63) that the acceleration is constant and equal to $2P/v_0 m_0$.

6.3 Constant I_{sp} Rocket Performance

By a similar process, the conventional rocket equation can be shown to be

$$v(t) = v_0 - u \ln \frac{1}{1 - \beta t} \tag{64}$$

where u is the exhaust velocity and β is defined by the equation

$$\beta \equiv \frac{m'}{m_0} \frac{m_f}{m_0 t} = \frac{\gamma}{t} \tag{65}$$

and where the mass flow rate m' is considered to be a constant. The integration of Eq. (64) yields the distance as a function of time,

$$\chi(t) = v_0 t + u \left[t + \frac{1 - \beta t}{\beta} \ln (1 - \beta t) \right] \tag{66}$$

and relating β to power through Eq. (48) one can use

$$\beta = \frac{2P}{u^2 m_0} . \tag{67}$$

Equations (65) and (67) can be combined to yield an expression for the exhaust velocity or I_{sp} in the case where it is a constant.

$$u = \left(\frac{2Pt}{m_0 \gamma} \right)^{1/2} . \tag{68}$$

16

6.4 Illustrative Examples

Two cases have been considered to compare a variable I_{sp} rocket to a constant I_{sp} one operating at the same power level.

First, consider a distance of 7.8×10^7 Km. as in a trip to the planet Mars, and consider two power levels: $P = .5$ MW and $P = 1.0$ MW. One inquires as to the total trip time for a rocket plus payload of 1.122×10^4 Kg delivered at the destination as a function of the total fuel on board. The analysis produces two times: t_c, from Eq. (66), which denotes the trip time for a constant I_{sp} rocket and t_h, from Eq. (63), which denotes that quantity for a hybrid plume rocket operating with its exhaust velocity optimally tuned in accordance with Eq. (49). The results are plotted in Fig. 7. Note that the solution of Eq. (63) gives only one point for a given value of P and hence, the two power levels under consideration here yield the two values of t_h shown in the graph. For t_c, on the other hand, the solution of Eq. (66) yields a continuous curve simply because one has flexibility in the m' and I_{sp} combination chosen to meet the power level requirement.

Note rom Fig. 7 that all the values of t_c are higher than the value of t_h at the corresponding power level. Additionally, decreasing or increasing the power level has a corresponding effect on trip time but does not change the relative comparison. There is a minimum trip time and hence, an optimum fuel mass for the constant I_{sp} rocket. given a payload and a power level. Physically, this means that too much fuel can significantly slow down the ship and too little means a very low acceleration for the trajectory. The hybrid plume, on the other hand, while using more fuel, insures that the acceleration is constant and trades off thrust for I_{sp} as the rocket velocity increases.

The second example is shown in Fig. 8 for a much longer trip and a smaller payload. The results are qualitatively the same: however, the gain in performance of the hybrid plume over the constant I_{sp} vehicle is much greater in this case.

These considerations show the fundamental advantage of variable I_{sp} propulsion. However, these results must be taken in the context of rectilinear motion in gravity-free space. The same analysis for the gravitational two-body problem of orbit transfer is now being

pursued by our research team. In principle, the important quantity to follow is the vehicle's state vector (i.e., velocity and position) with respect to the Earth (if the fuel is loaded there). Under these circumstances, the relative velocity of the rocket may vary from a low value at apogee to a high value at perigee or gradually decrease as the vehicle spirals out. The control law for the operation of the engine may be different in form; nevertheless, variable I_{sp} propulsion will probably yield substantial advantages in this realm as well.

7.0 Experimental Facility

The purpose of this work is to investigate the basic physics of the small tandem mirror device. The goal is to establish a generic tandem mirror plasma facility suitable for investigating the hybrid plume and other high power variable I_{sp} plasma propulsion concepts [1,2,3].

The tandem mirror design is shown in Figs. 1 and 3 and has the following major components: the magnetic containment coils, the vacuum vessel, a cold plasma injector at the closed end, an rf antenna for ion cyclotron resonance heating (ICRH) and capability for a hybrid plume exhaust at the open end. The plasma is injected by a gun and heated to a few 100 eV in the central cell by ICRH. The hybrid plume can be produced by injecting a hypersonic, coaxial gas jet at the exhaust end which partially mixes with the hot plasma to produce thrust. The exhaust can be controlled by a combination of varying the injector current, the electric potential in the anchor, the magnetic field and gas jet stagnation pressure. During the design phase it was decided to quadruple the magnetic field intensity reported previously [4] to increase confinement time. This was done with minor changes to the coil configuration. The design of a cryogenic coil system, vacuum vessel and structure were kept as simple as possible. Alignment is minimal. Initially, only the central cell, booster coil and mirror coils will be required. The Ioffe and saddle coils will be added later. Ingenious design and fabrication methods have been devised to facilitate a drastic saving in fabrication costs. Table I lists the major parts for the device, the parts being built, and the parts deferred for future upgrade. The central coils and one mirror coil have been delivered and electrical tests have been performed. The waveform of the tests

is shown in Fig. 4. The mirror coil has been energized up to 1000 amp for up to 1 sec time duration without cooling. The true values of inductance and resistance are also measured. The assembly will begin in the fall. The objectives of this experiment are listed in Table II and are also discussed below.

(a) Plasma containment, replenishment, and exhaust

The bulk plasma will be generated by rf breakdown of gaseous hydrogen in one of the closed mirror end or in the central cell. The central cell plasma buildup will be observed and the exhaust through the other end will be measured. Tuning of the magnetic field coils and electric plug potential profile will be performed to obtain the best grade central plasma and the most useful exhaust. Means of plasma replenishment such as central cell gas injection, a gas blanket, pellet injection, and streaming gas from the closed end will be investigated. The effect of these replenishing methods on the exhaust properties at both low and high particle confinement times, will be the center of interest.

(b) Plasma heating

Plug and central cell plasma heating by ion cyclotron resonance heating (ICRH) will be used. The efficiency of this energy injection method is highly dependent on antenna design and magnetic field shaping. Accordingly, a major objective of this research is to optimize the antenna design for this particular application and investigate the operational regimes and power levels which can be achieved. Other forms of energy loss, such as radiation and charge exchange affecting the overall power balance, will be measured as well.

(c) Stability and control

One of the major objectives of this experiment is to generate stable and well-behaved plasmas over as large a set of operating conditions as possible for the compact device. A great deal of existing experimental knowledge and raw data, derived from similar fusion experiments will be utilized here to achieve the best plasma operation under varying conditions. This will become useful later, in future experiments with variable I_{sp} exhausts. Clearly then, stability and control of the plasma will be an important area of investigation.

19

Moreover, the very fact that a preferential flow direction exists in this case will mean a certain asymmetry in the configuration of the machine in the longitudinal direction. The effects of such asymmetries on plasma stability will be investigated.

The bulk of the experimental data will be integrated in the form of an "operational envelope" map for this device. Such a map will continue to be ref...ed as more experience is gained and will form the basis for the next phase, where a wide variety of high thrust, variable I_{sp} rocket experiments will be investig...ed.

(d) Instrumentation

A control system will be developed to achieve high reproductivity of the plasma and exhaust properties with minimum monitoring for reliable operation.

References

1 Chang, F. R., Fisher, J. L., Nucl. Fus. **22** (1982).

2 Chang, F. R., Krueger, W. A., Yang, T. F., Fisher, J. L., "Plasma-Gas Interaction Study in a Hybrid Plume Plasma Rocket". AFOSR/AFRPL Chemical Rocket Research Meeting, paper 51, Lancaster, CA, March 1985.

3 Chang, F. R., Kureger, W. A., Yang, T. F., "Numberical Modeling of the Hyrid Plume Plasma Rocket", AFOSR/AFRPL Chemical Rocket Research Meeting, paper 30, Lancaster, CA, September 1986.

4 Chang, F. R., Krueger, W. A., Yang, T. F., AIAA/DBLR/JSASS Int. Electric Propulsion Conf., paper AIAA-85-2049, Alexandria, VA, September 1985.

5 Yang, T. F., Miller, R. H., Wenzel, K. W., Krueger, W. A., AIAA/DBLR/JSASS Int. Electric Propulsion Conf., paper AIAA-85-2054, Alexandria, VA, Sept. 1985.

6 Yang, T. F., Chang-Diaz, F. R., Peng, S. Y., Krueger, W. A., AFOSR AFRPL Chemical Rocket Res. Mtg., paper 29, Lancaster, CA (1986).

TABLE I

Major Parts	Parts Being Built	Parts for Upgrade
Central Cell Coils	Central Cell Coils	
Vacuum Chamber	Vacuum Chamber	
Booster Coils	Booster Coils	
Saddle Coils		Saddle Coils
Ioffe Coils		Ioffe Coils
RF Transmitter and Antenna	RF Transmitter and Antenna	

TABLE II

Experimental Objectives

1. Plasma containment.

   RF breakdown of hydrogen gas.

   Central plasma buildup.

   Scanning of magnetic field and electric plugging field for best grade central plasma.

2. Plasma Heating.

   Plug and central cell plasma heating by ion cyclotron resonance heating method.

   Optimize heating efficiency.

3. Stability Control.

   Generate stable and well-behaved plasmas over a large set of operating conditions.

4. Instrumentation

   Minimize instrumentation.

5. Thrust and I_{sp} study.

Ioffe coil

Booster coils

Central cell coils

Saddle coils

Ioffe coil

Mirror coils
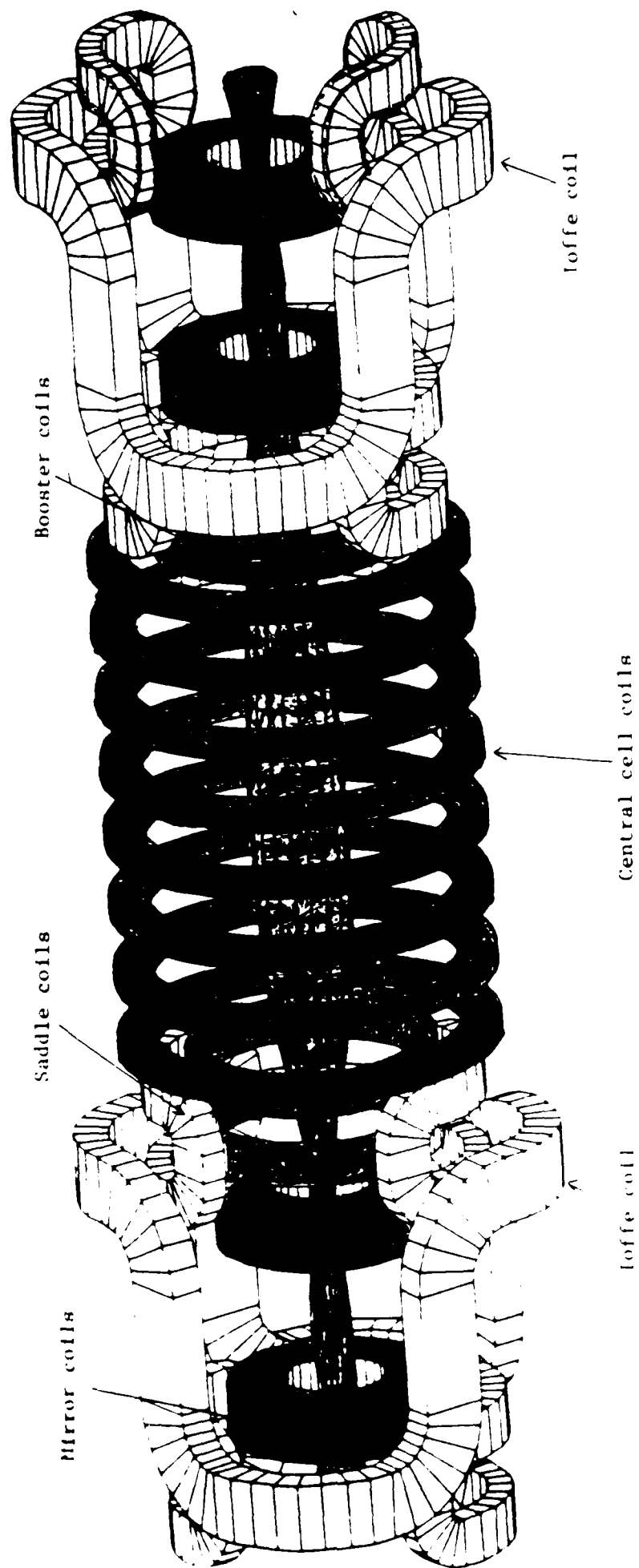
Figure 1: Trimetric view of the tandem mirror plasma source showing plasma shape and exhaust.
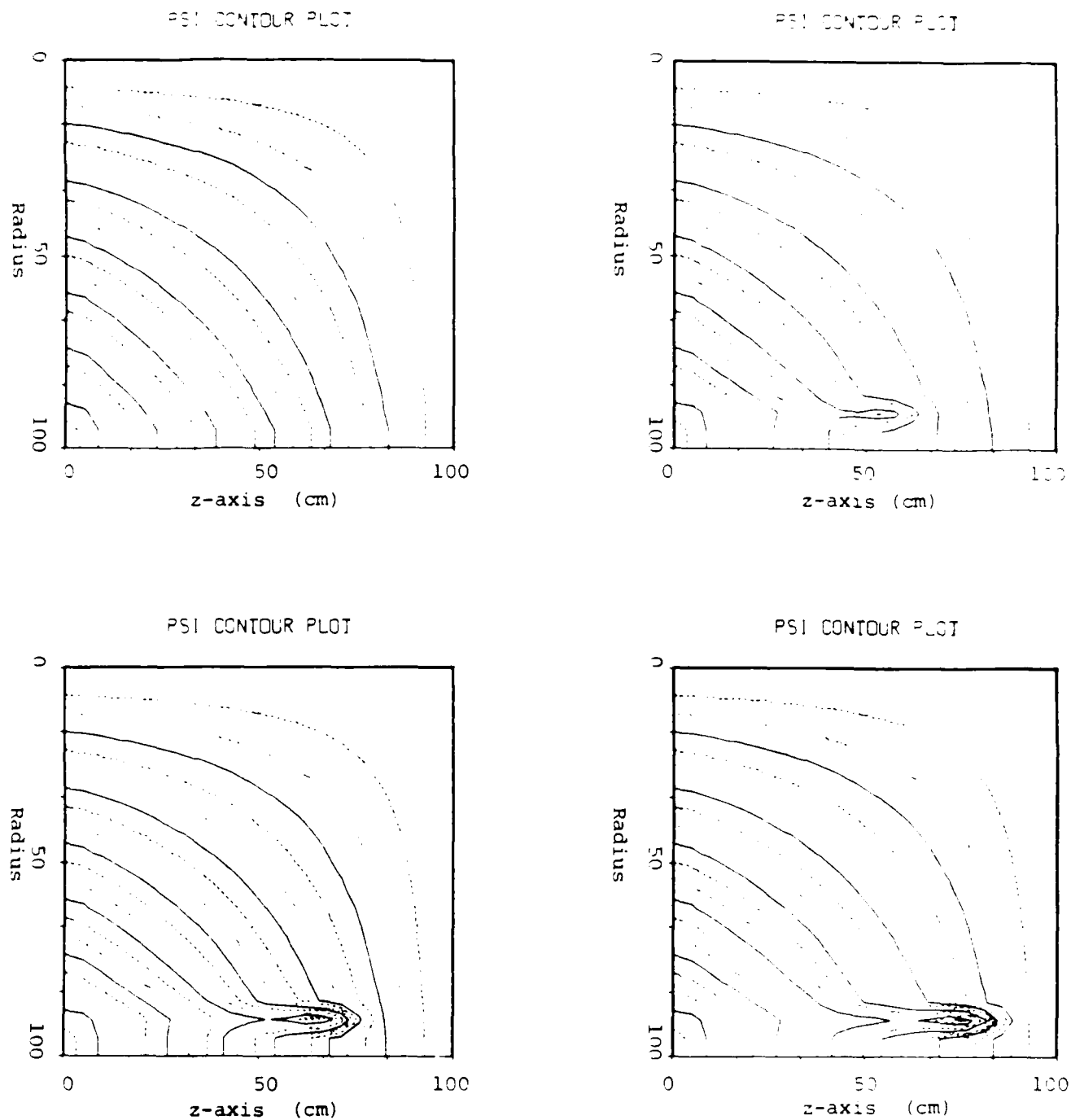
Figure 2

Magnetic field lines with neutral gas jet near wall (symmetry line at the top of each plot). Neutral gas is "ionized" at 40cm down duct, and momentum pushes field lines/plasma down duct. The flow in these figures is not self consistent, but represent the ideal fluid flow possible. (1a) Initial field configuration. (1b) Island (or "smoke ring") begins to form. (1c) Island breaks away. (1d) Island continues to move down duct, disconnected from nozzle.
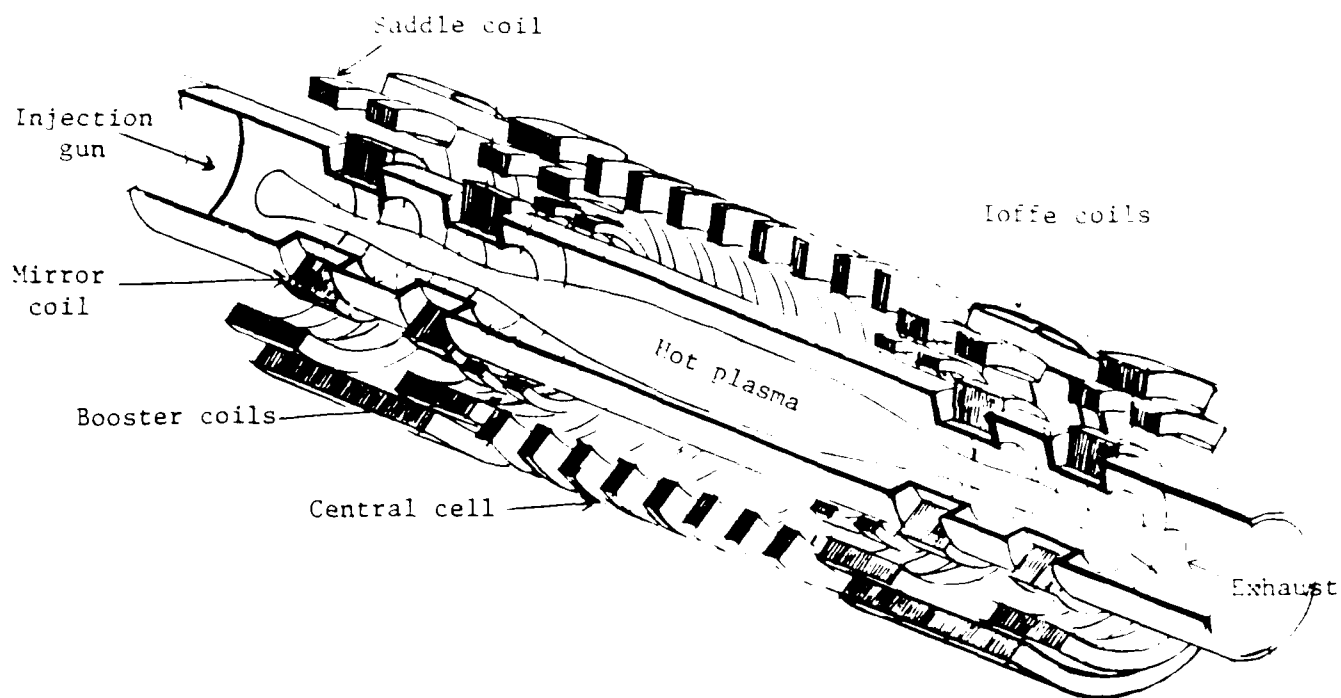
Saddle coil

Injection
gun

Ioffe coils

Mirror
coil

Hot plasma

Booster coils

Central cell

Exhaust

Diagnostic port

Ioffe coil housing
(cryogenic)

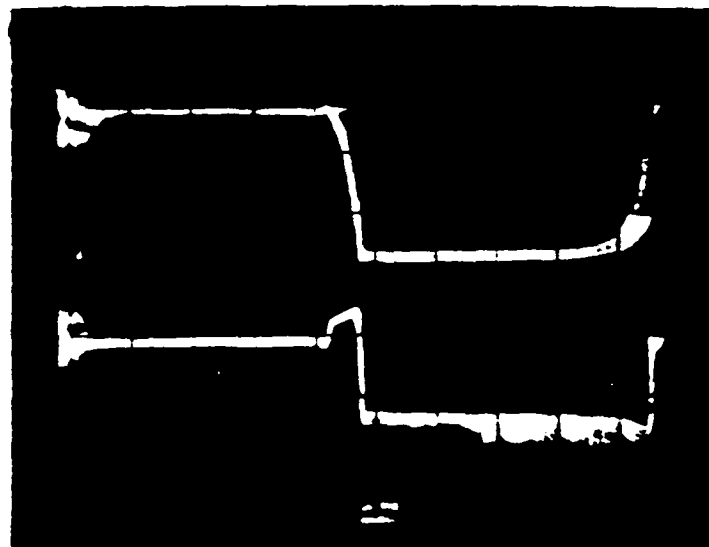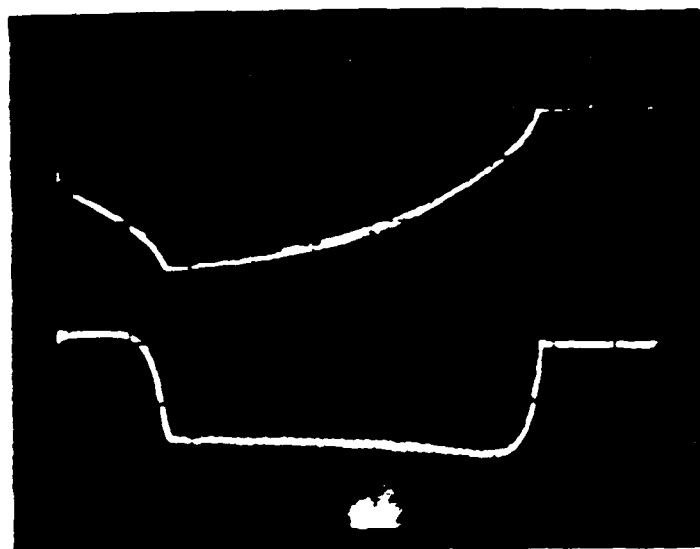Vacuum chamber

Support

Pumping port
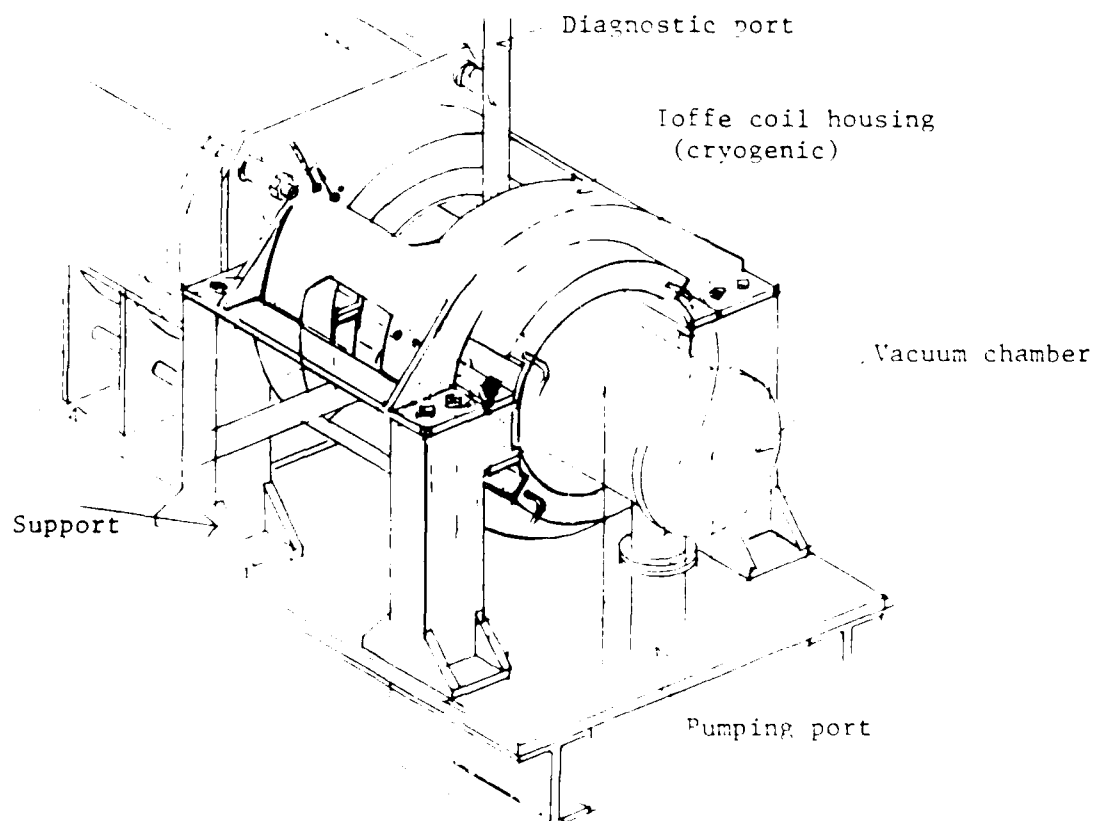
Figure 3: Tandem mirror assembly and experimental setup.

(a)

5 Volts

220 amp

1 sec

(b)

2 Volts

82 amp

1 sec

Inductance   3 mh

Resistance (room temp)   30 m ohm

Figure 4:   Typical voltage (upper curve) and current (lower curve)
traces for energizing the central cell coil at
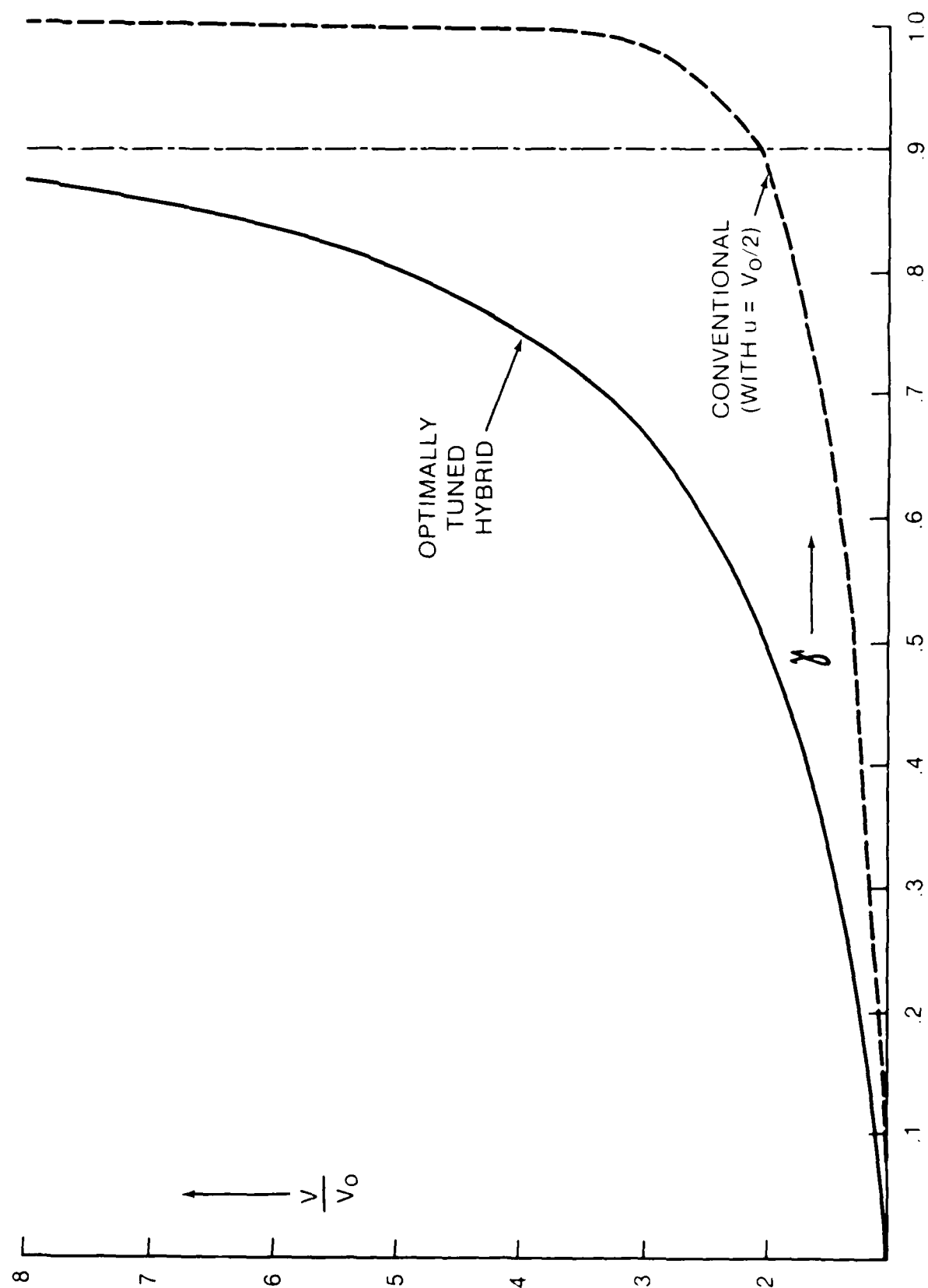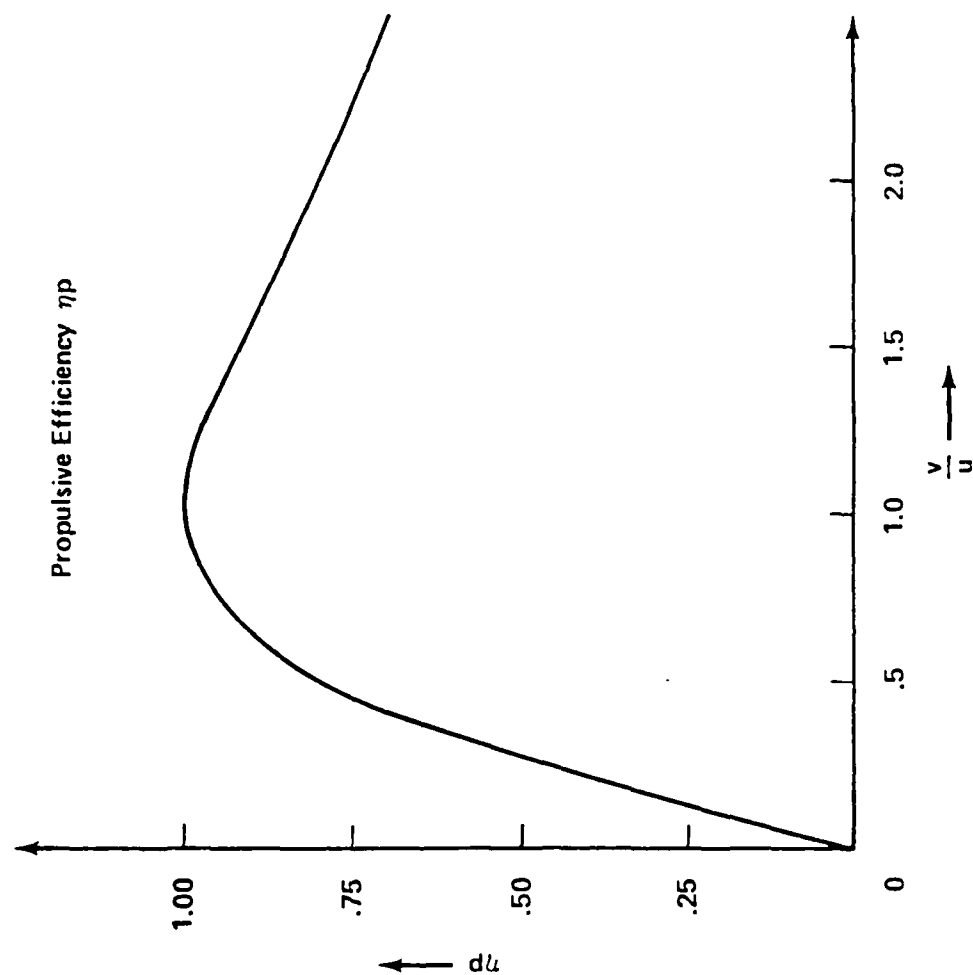(a) 220 amp and (b) 82 amp.

Figure 5

Propulsive Efficiency ηp

u = Exhaust Velocity
v = Vehicle Velocity

$$\eta p = \frac{2\,(v/u)}{(\frac{v}{u})^2 + 1}$$

Figure 6

Figure 7

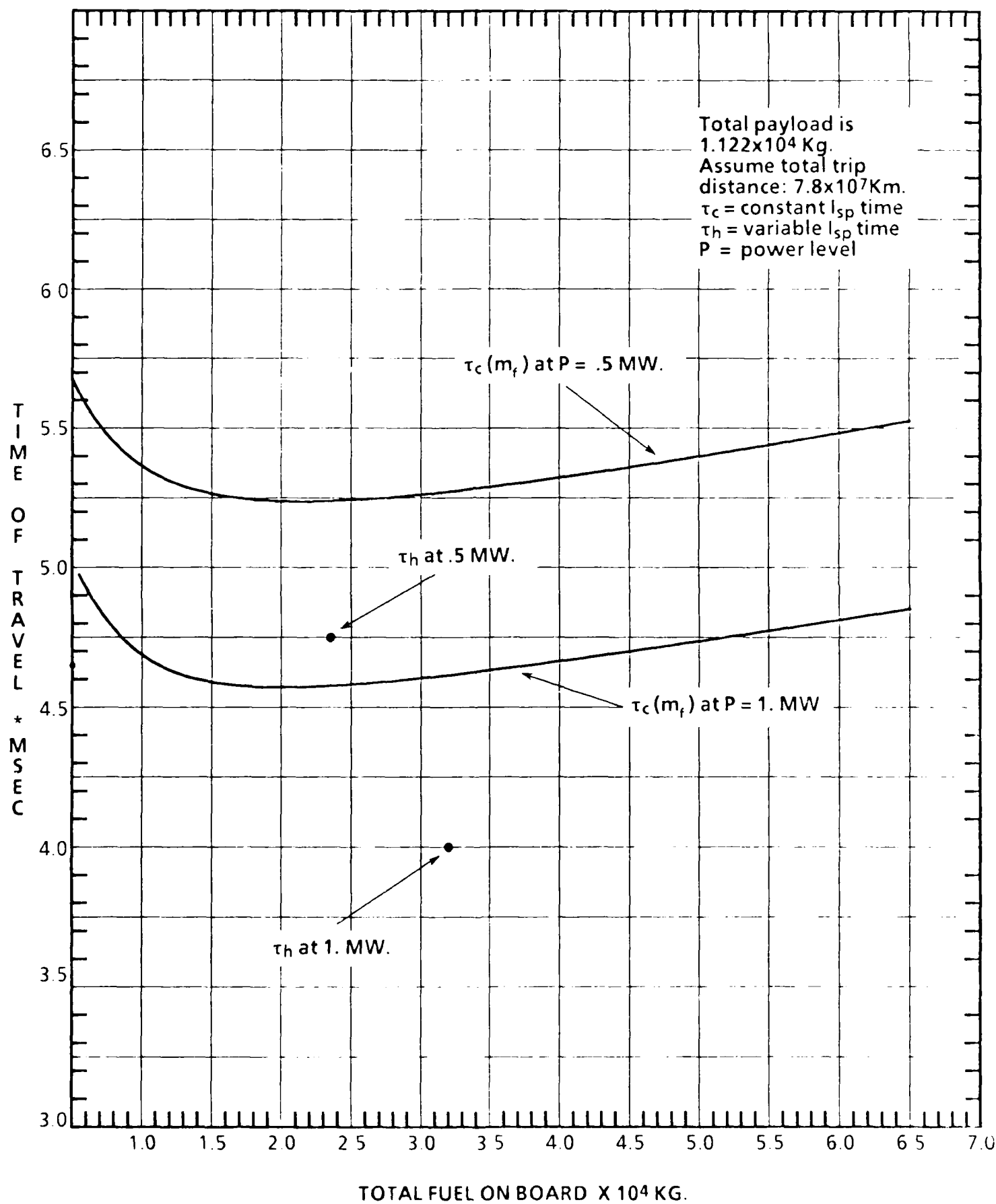# Variable vs Constant I_{sp} Rocket performance comparison

$\tau_c(m_f)$ at P = .5 MW.

Total payload is
3.401×10^3 Kg.
Assume total trip
distance: 2.3×10^8 Km.
τ_c = constant I_{sp} time
τ_h = variable I_{sp} time
P = power level

$\tau_c(m_f)$ at P = 1. MW

τ_h at .5 MW.

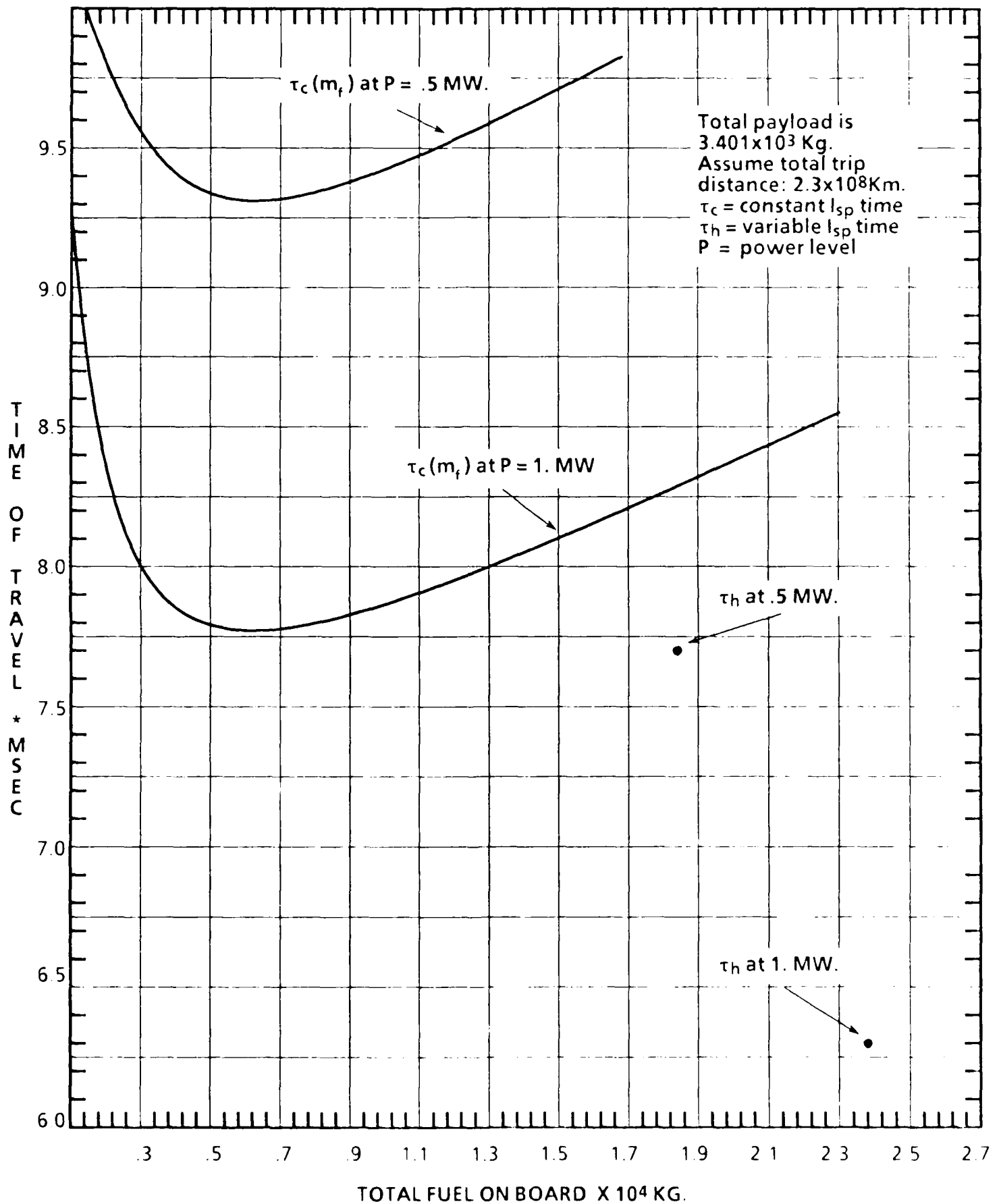τ_h at 1. MW.

TIME OF TRAVEL * MSEC

TOTAL FUEL ON BOARD X 10^4 KG.

Figure 8

END

DATE

FILMED

DTIC

4/88